Acta Geologica Polonica, Vol. 74 (2024), No. 3, e20
DOI: 10.24425/agp.2024.151750

Titanite from the NYF-type pegmatites of Szklarska Poręba Huta quarry, Karkonosze granite massif, SW Poland

KAROLINA MIL, BOŻENA GOŁĘBIOWSKA, ADAM PIECZKA and ADAM WŁODEK

Department of Mineralogy, Petrography and Geochemistry, AGH University of Krakow, Mickiewicza 30, 30-059 Kraków, Poland;
e-mails: mil@agh.edu.pl; goleb@agh.edu.pl; pieczka@agh.edu.pl; wlodek@agh.edu.pl

ABSTRACT:

Mil, K., Gołębiowska, B., Pieczka, A. and Włodek, A. 2024. Titanite from the NYF-type pegmatites of Szklarska Poręba Huta quarry, Karkonosze granite massif, SW Poland. *Acta Geologica Polonica*, **74** (3), e20.

Titanite, an accessory mineral of pegmatite related to aplogranite, was identified in the Szklarska Poręba Huta quarry within the Karkonosze granite massif in Lower Silesia, Poland. It formed during pegmatitic to hydrothermal stages. Besides the isovalent substitution Sn → Ti, the chemical composition of the mineral is characterized by three coupled substitutions: (1) $(Al, Fe, Sc)^{3+} + (OH, F)^{-} \rightarrow {}^{Y}Ti + {}^{Z}O$, (2) $^{X}REE^{3+} + {}^{Y}(Al, Fe, Sc)^{3+} \rightarrow {}^{X}Ca^{2+} + {}^{Y}Ti^{4+}$, and (3) $(Al, Fe, Sc)^{3+} + (Nb, Ta)^{5+} \rightarrow 2^{Y}Ti$. These substitutions are strongly dependent on the composition of the magma in terms of its Al_2O_3/TiO_2 activity ratio, with the first one also influenced by the H_2O/HF fugacity ratio. Fluorine, which induced the most common substitution (1), had its source in high-temperature F-bearing fluids released from rocks of the metamorphic envelope adjacent to the intruding granite. These fluids mobilized and transported various rock components (Sc, REE, Nb, Ta, etc.) among others in the form of fluoride complexes, enriching the aplogranite magma with some metallic elements. The substitution of Sn for Ti developed with decreasing temperature to the extent that in thin ore-mineralized quartz veins cutting aplogranite, titanite reaches Sn-bearing compositions up to the prevalence of Sn corresponding to malayaite.

Key-words: Titanite; Malayaite; NYF pegmatite; Karkonosze granite massif; Szklarska Poręba.

INTRODUCTION

Currently, an informal titanite group comprises five different mineral species: titanite $CaTi(SiO_4)O$ (grandfathered), malayaite $CaSn(SiO_4)O$ (Alexander and Flinter 1965; Higgins and Ribbe 1977), vanadomalayaite $CaV^{4+}(SiO_4)O$ (Basso *et al.* 1994), natrotitanite $(Na_{0.5}Y_{0.5})Ti(SiO_4)O$ (Stepanov *et al.* 2012), and żabińskiite, $Ca(Al_{0.5}Ta_{0.5})(SiO_4)O$ (Pieczka *et al.* 2017). The chemical formulae of these minerals can be generalized as $XYTO_4Z$, where the symbol X denotes a 7-fold-coordinated site commonly occupied by Ca, which can be partially replaced by small amounts of cations with large radii, e.g. Na^{+}, Mn^{2+}, Sr^{2+}, Pb^{2+}, REE^{3+}, Th^{4+}, U^{4+}; Y – an octahedral site usually occupied by Ti^{4+}, which can be substituted by common di- and trivalent cations such as Mg^{2+}, Fe^{2+}, Mn^{2+}, Al^{3+}, Fe^{3+}, Mn^{3+}, in addition to other (besides Ti^{4+}) high-field-strength elements (HFSE: V^{4+}, Sn^{4+}, Zr^{4+}, Nb^{5+}, Ta^{5+}); T – a tetrahedral site occupied mainly by Si^{4+}, and in the deficiency of Si^{4+} completed by subordinate Al^{3+} or Ti^{4+}; Z – an anionic site that, in addition to O^{2-} anion, can contain $(OH)^{-}$, F^{-}, and Cl^{-} (e.g. Zachariasen 1930; Černý and Riva di Sanseverino 1972; Clark 1974; Higgins and Ribbe 1976; Speer and Gibbs 1976; Ribbe 1980; Černý *et al.* 1995; Della Ventura *et al.* 1999; Tiepolo *et al.* 2002; Chakhmouradian *et al.* 2003; Cempírek *et al.* 2008). The highly diverse compositions of the group minerals are the result of an extensive stability field that is slightly dependent on the composition of the evolving parental magmatic systems and the kinetics of crystallization (Franke and

© 2024 Karolina Mil, Bożena Gołębiowska, Adam Pieczka, and Adam Włodek. This is an open access article under the CC BY license (http://creativecommons.org/licenses/by/4.0/), which permits use, distribution, and reproduction in any medium, provided that the article is properly cited.

Ghobarkar 1980; Brugger and Gieré 1999; Liferovich and Mitchell 2005). Magmatic titanite typically has a composition close to the end-member constituent, with only minor substitutions.

The structure of titanite is formed by $[^{Y}TiO_6]$ octahedra chains linked by isolated $[^{T}SiO_4]$ tetrahedra, forming a framework of $[TiOSiO_4]$, which encloses $^{X}Ca^{2+}$ in irregular 7-fold coordination. At room temperature, titanite crystallizes in the monoclinic $P2_1/a$ space group, but with significant substitutions at the Y or X + Y sites a phase transition results in transformation to the monoclinic $A2/a$ space group (Higgins and Ribbe 1976; Speer and Gibbs 1976; Bismayer *et al.* 1992; Zhang *et al.* 1995; Meyer *et al.* 1996; Kek *et al.* 1997; Beirau *et al.* 2014). Additionally, a triclinic *A*-1 structure has been observed in Ta- and Nb-enriched titanite from the Heftetjern pegmatite in Tørdal, southern Norway (Lussier *et al.* 2009), and in holotype żabińskiite from the Piława Górna pegmatite in Poland (Pieczka *et al.* 2017).

In this paper, we describe titanite of post-magmatic evolutionary stages (pegmatitic to hydrothermal) in the Karkonosze granite exposed in Szklarska Poręba Huta quarry. Our studies focus on the evolution of the mineral in order to better understand the processes leading to its compositional heterogeneity.

GEOLOGICAL SETTING

The Karkonosze granite massif, located in the Western Sudetes of Poland, lies at the northeastern margin of the Bohemian Massif. It represents a fragment of the Central European Variscides, formed during multi-stage collision events and related metamorphic episodes (e.g., Berg 1913; Petrascheck 1933; Kozłowski *et al.* 1975; Kozłowski 1978; Aleksandrowski and Mazur 2002; Mazur *et al.* 2006; Mikulski 2007; Ilnicki 2011). The massif consists of a Carboniferous-age granite intrusion, extending for approximately 70 km from east to west. It is bounded by Jelenia Góra to the northeast, Kowary to the south, and follows the Polish-Czech boundary westward to Liberec in the Czech Republic (Text-fig. 1). The pluton formed ~312–315 Ma ago (Duthout *et al.* 1991; Machowiak and Armstrong 2007; Žák *et al.* 2013; Kryza et al. 2014 a, b; Kusiak *et al.* 2014; Mikulski *et al.* 2020)), on the active margin of a crystalline continental platform adjacent to oceanic crust, from granitic magmas in the temperature range of 990–840°C (Kozłowski 2007). It is considered to be a syn-collisional magmatic arc intrusion originating from relatively reduced magmas that underwent complex evolution (Duthou *et al.* 1991; Kröner *et al.* 1994; Mikulski 2007; Słaby and Martin 2008; Kryza *et al.* 2014 a, b; Kozłowski *et al.* 2016). The Karkonosze granite massif is composed of three lithological varieties: central / porphyritic granite, ridge / equigranular granite, and granophyric granite / aplogranite (Borkowska 1966). These varieties are related to mixed crustal- and mantle-derived, highly-developed magmas of K-rich, calc-alkaline to subalkaline I-type and transitional I/S type (Wilamowski 1998; Oberc-Dziedzic *et al.* 1999; Mazur *et al.* 2007; Mikulski 2007; Słaby and Martin 2008). The pluton is hosted by a Neoproterozoic–Palaeozoic cover consisting of four distinct structural units: the Izera-Kowary Unit, Ještěd Unit, Southern Karkonosze Unit, and Leszczyniec Unit. These units are interpreted as elements of a nappe structure that underwent Variscan regional metamorphism and contact metamorphism during the intrusion of the Karkonosze granite massif (Kryza and Mazur 1995; Mazur and Aleksandrowski 2001; Aleksandrowski and Mazur 2002).

The Karkonosze granite massif is characterized by post-magmatic activity, evidenced by small polymetallic deposits located in the contact aureole of the granite, and by numerous intra-granitic pegmatites. The pegmatites usually form zoned pods, small lenses and, more rarely, dykes of sizes up to several decimeters, exceptionally reaching several meters. In the past, they were mined for feldspar as raw material for the local ceramic industry. The origin of the pegmatites is related to the crystallization of late granitic magmas rich in volatiles followed by the hydrothermal-metasomatic recrystallization of the primary granite at a temperature range from 560 to 160–90°C (Kozłowski 1978; Kozłowski and Sachabiński 2007; Kozłowski *et al.* 2016). Decreasing temperature and variations in pH, Eh, S, and fO_2 of the highly-fractionated parental magma-fluid system with increased abundance of metallic elements (Mikulski 2007) also resulted in the deposition of small amounts of ores, mined in the past as local polymetallic deposits. Signs of such mineralization extend across a considerable distance, especially near the granitic metamorphic rocks of the Kowary-Izera Unit in the eastern metamorphic cover, e.g., the Miedzianka-Ciechanowice area, Rędziny, Czarnów, Kowary, Budniki, and Sowia Dolina, as well as to the northern metamorphic cover of the Izera region, e.g. Przecznica, Gierczyn, Krobica, Czerniawa (for details see Mochnacka *et al.* 2015).

The Szklarska Poręba-Huta quarry is the only active locality in the Polish part of the massif for the ex-

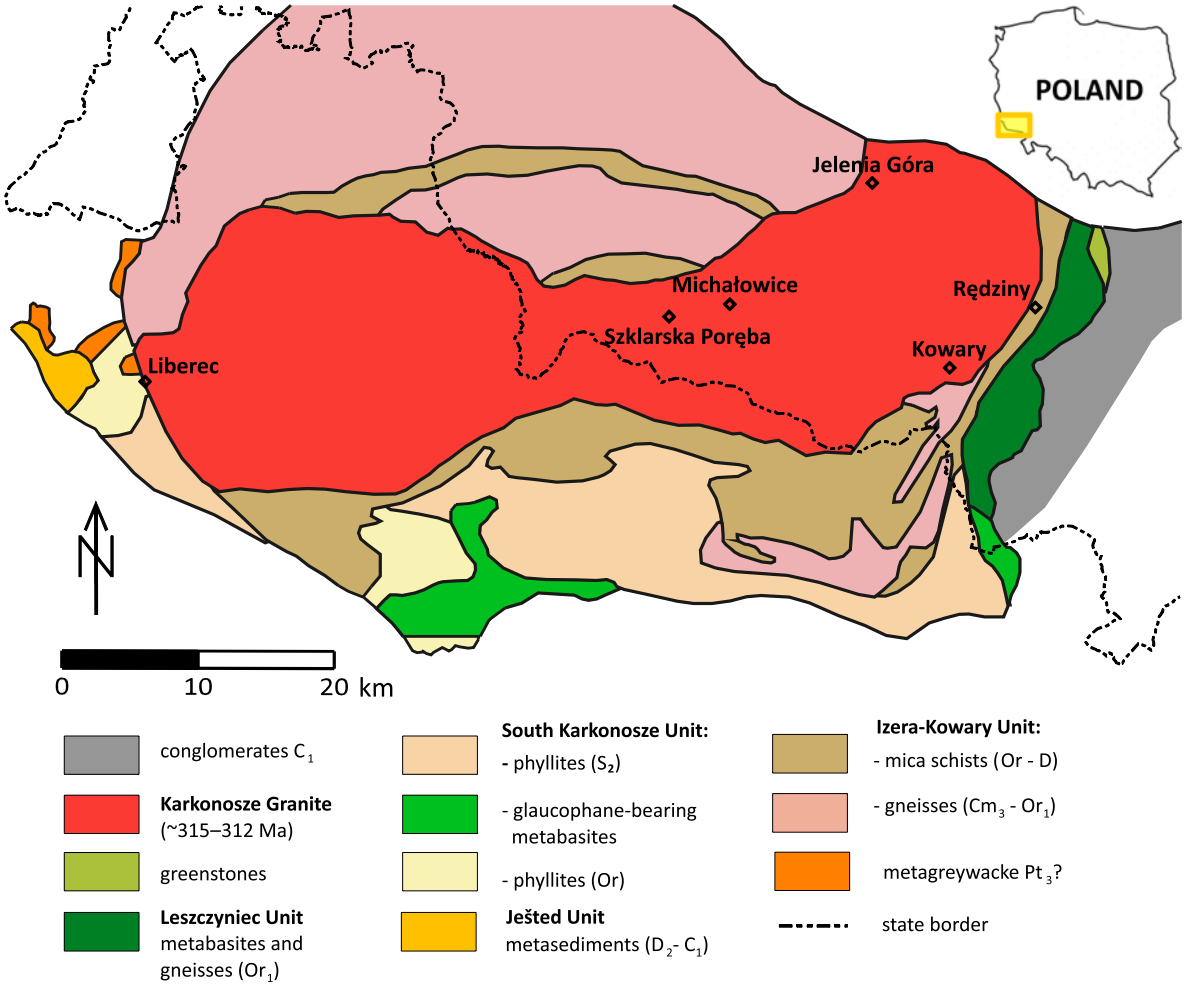

Text-fig. 1. Geological sketch map of the Karkonosze-Izera Massif (modified after Mazur 1995; Majka *et al.* 2018).

ploitation of Karkonosze granite. It is known for its diverse W-Sn-Mo-Bi and Th-U-REE associations with Nb- and Sc-bearing phases occurring in the NYF-type pegmatite, quartz veins, and aplogranite (e.g., Gajda 1960; Karwowski *et al.* 1973; Kozłowski and Karwowski 1975; Olszyński *et al.* 1976; Pieczka and Gołębiowska 2002; Pieczka *et al.* 2003, 2022, 2023; Mikulski *et al.* 2004; Mikulski 2007; Kozłowski and Sachabiński 2007; Pieczka and Gołębiowska 2012; Kozłowski *et al.* 2016; Evans *et al.* 2018; Kozłowski and Matyszczak 2018). The wolframite-scheelite-cassiterite mineralization started to crystallize during the final stage of pneumatolytic processes and was successively developed during a hydrothermal stage. It is associated with a sulphide assemblage represented by molybdenite, pyrite, chalcopyrite, pyrrhotite, sphalerite, emplectite, nuffieldite, bismuthinite, marcasite, bismuth, some supergene minerals, and rare Bi sulphides and sulphosalts, as aikinite series, cuprobismutite homologues, galenobismutite, cannizzarite, cosalite, ikunolite, and joséite-A. The crystallization sequence of the mineral assemblage was determined to be: magnetite 525–465°C, wolframite 520–390°C, cassiterite 515–470°C, molybdenite 455–390°C, sphalerite 415–390°C, bismuthinite 270–245°C, and bismuth about 265 and 135°C (Kozłowski *et al.* 2002). In addition, ilmenite, pyrophanite, hematite, titanite, malayalite, zircon, epidote, pumpellyite-(Mg), pumpellyite-(Fe), clinochlore, chamosite, laumontite, chabazite and stilbite have been recognized in the locality. The post-magmatic Th-U-REE assemblage is represented by numerous REE-bearing phases, e.g., xenotime-(Y), monazite-(Ce), allanite-(Ce), yttrialite-(Y), gadolinite-(Y), gadolinite-(Ce) and hingganite-(Y); Nb-bearing phases by fergusonite-(Y) or fergusonite-(Y)-beta, columbite-(Fe), fersmite; and

Sc-bearing phases by thortveitite, nioboheftetjernite, scandian columbite-(Fe) and rare sorosilicates: kristiansenite, kozłowskiite, and silesiaite; all of which contain Sc.

METHODS

Electron-probe micro-analysis (EPMA) was carried out in wavelength dispersive spectroscopy (WDS) mode using a JEOL SuperProbe JXA-8230 instrument at the Laboratory of Critical Elements AGH-KGHM (AGH University of Krakow, Poland). Small fragments of pegmatite, mineralized quartz veins, and host granite from the Szklarska Poręba Huta quarry were embedded in epoxy, prepared as 1-inch discs, then polished and coated with carbon. The following analytical conditions were applied: acceleration voltage 15 kV; beam current 40 nA, peak-count time 10–20 s, and 40 s for U, Pb, Sc, and HREE; beam diameter 2–3 μm. Backscattered electron (BSE) images were acquired under identical operating conditions. The standards, analytical lines, diffraction crystals, and mean detection limits (element wt.%) used were as follows: F – fluorite (*K*α, TAPH, 0.07), Na – albite (Kα, TAP, 0.01), Mg – diopside (*K*α, TAPH, 0.02), Al – albite (*K*α, TAPH, 0.03), Si – albite (*K*α, TAP, 0.03), Ca – diopside (*K*α, PETJ, 0.02), Sc – metallic Sc (*K*α, PETJ, 0.02), Ti – rutile (*K*α, PETJ, 0.03), V – vanadium (*K*α, PETJ, 0.03), Mn – rhodonite (*K*α, LIFL, 0.02), Fe – hematite (*K*α, LIFL, 0.02), Y – YPO_4 (*L*α, PETJ, 0.03), Zr – zircon (*L*α, PETJ, 0.05), Nb – $LiNbO_4$ (*L*α, PETJ, 0.06), Sn – cassiterite (*L*α, PETJ, 0.02), Ce – $CePO_4$ (*L*α , LIF, 0.05), Gd – $GdPO_4$ (*L*β, LIFH, 0.08), Dy – $DyPO_4$ (*L*α, LIFH, 0.04), Ho – $HoPO_4$ (*L*β, LIFL, 0.06), Er – $ErPO_4$ (*L*α, LIFH, 0.05), Tm – $TmPO_4$ (*L*α, LIFL, 0.05), Yb – $YbPO_4$ (*L*α, LIFL, 0.05), Lu – $LuPO_4$ (*L*α, LIFH, 0.06), Ta – manganotantalite (*L*α, LIFH, 0.09). W, La, Ce, Pr, Nd, Sm, Eu, Tb, Pb, U, Th were below the respective detection limits. Raw data were reduced using the ZAF routine (Z – atomic number, A – absorption, F – fluorescence). This set of EPM analyses was supplemented by several unpublished analyses of Sn-bearing titanites previously performed by one of the authors (AP) in a specimen SP5 containing the holotype for silesiaite and kozłowskiite (Pieczka *et al.* 2017, 2022, 2023). The empirical formulae of titanite were normalized with respect to three X + Y + T atoms per formula unit (pfu). The content of H_2O, present in titanite in the form of OH^- groups, was calculated based on the stoichiometry of the titanite-group minerals assuming Fe_{total} is Fe^{3+}.

CHEMICAL COMPOSITION OF THE SZKLARSKA PORĘBA HUTA TITANITES

Text-figure 2 shows representative backscattered electron (BSE) images of mineral aggregates from pegmatites of the Szklarska Poręba Huta quarry, where titanite occurs. Individual grains of the mineral vary in sizes, ranging from hundredths of micrometers to 1–1.2 millimeters. They are usually intensively zoned, with the most common patterns being oscillatory and mosaic, and less commonly irregular patchy zoning. Typical associated minerals with titanite include common minerals such as bismuth, bismuthinite, cassiterite, pyrite, chalcopyrite, rutile, ilmenite, pyrophanite, scheelite, scolecite, and chlorite, as well as rarer phases such as stokesite $CaSnSi_3O_9 \cdot 2H_2O$, and hingganite-(Y) $(Y,REE,Ca)_2(\square,Fe^{2+})Be_2[SiO_4]_2(OH)_2$. Representative EPMA analyses of titanite are summarized in Table 1.

In titanites, the X site is dominantly occupied by Ca (23.60–29.62 wt%; 0.848–1.008 Ca apfu) and supplemented by Y (0.00–6.83 wt% Y_2O_3; 0.000–0.122 Y apfu) and lanthanides (0.00–2.47 wt% Ln_2O_3; 0.000–0.026 Ln apfu), mainly represented by heavy rare-earth elements (HREE). Sodium was noted only in crystals of Sn-bearing titanite and malayaite from specimen SP5 (0.13–0.64 wt% Na_2O; 0.006–0.028 Na apfu). However, despite their maximum Y_2O_3 content of 0.07 wt% (0.001 Y apfu) and Ce_2O_3 of 0.14 wt% (0.001 Ce apfu), these crystals exhibited minimal REE. A co-variation (in apfu) of REE *versus* Ca (Text-fig. 3A) is described by the equation $REE = -0.916 \cdot Ca + 0.917$ ($R^2 = 0.976$). Due to the heterovalent nature of this substitution, the resulting charge excess must be balanced by a substitution in another structural site. This is only possible in the coupled substitution $^{X}Ca^{2+} + {}^{Y}Ti^{4+} = {}^{X}REE^{3+} + {}^{Y}(Al, Fe, Sc)^{3+}$ at the X and Y sites (Text-fig. 3A). Text-figure 3B shows the relationships between $^{X}REE^{3+}$ and $^{Y}(Al, Fe, Sc)^{3+}$. For some analytical spots, the increasing content of ^{X}REE together with the increase of trivalent Y-site occupants $(Al, Fe, Sc)^{3+}$ reaches the limit value indicated by the ^{X}REE / $^{Y}(Al, Fe, Sc)^{3+}$ ratio of 1:3. The ratio corresponds to the substitution: $REE(Al, Fe, Sc)^{3+}{}_3(F, OH)_2\ Ca_{-1}Ti_{-3}O_{-2}$, indicating that at most ~1/3 of the total $^{Y}(Al, Fe, Sc)^{3+}$ is involved in this replacement. All data points below the 1:3 line indicate titanite spots where this substitution becomes negligible due to the absence of REE in the crystallization environment.

The Y-site occupation is more heterogeneous. Typically, predominant in this site is Ti (17.00–34.53 wt% TiO_2; 0.458–0.846 Ti apfu), with lower Ti con-

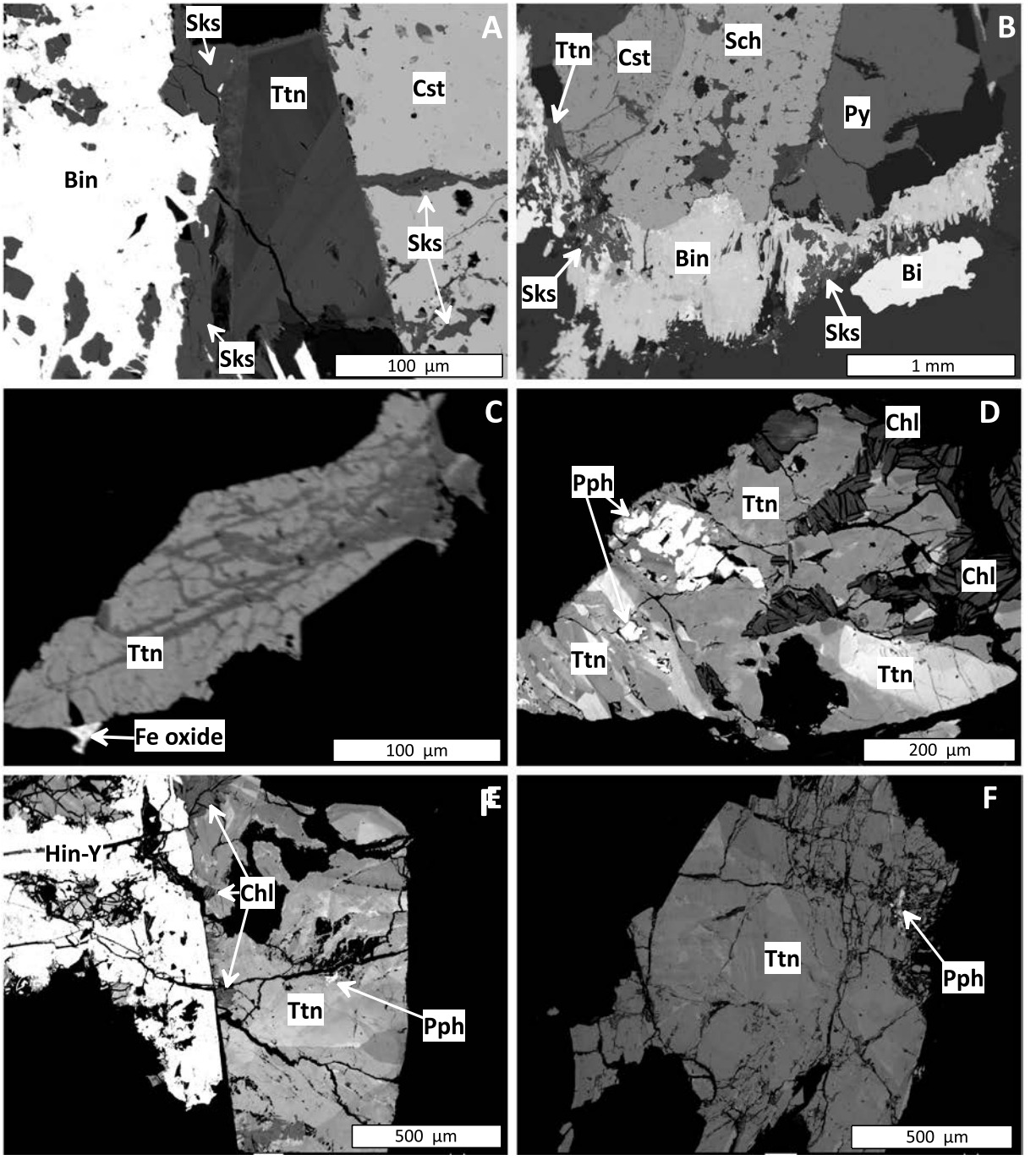

Text-fig. 2. Representative BSE images of titanite crystals from the Szklarska Poręba Huta pegmatites: (A) subhedral titanite with distinct patchy zoning; (B) Sn- and Bi-bearing ore mineralization associated with titanite; (C) anhedral titanite in matrix of the rock-forming minerals; (D) titanite crystal with pyrophanite inclusions overgrown by chlorite; (E) titanite associated with hingganite-(Y); (F) anhedral titanite with weak zoning pattern. Mineral symbols: Bi – bismuth, Bin – bismuthinite, Chl – chlorite; Cst – cassiterite, Hin-Y – hingganite-(Y), Pph – pyrophanite; Py – pyrite, Sch – scheelite, Sks – stokesite; Ttn – titanite. The abbreviations are after Warr (2021)

tents only in the specimen SP5 (11.18–18.83 wt% TiO_2; 0.341–0.529 Ti apfu). Titanium is typically substituted by other tetravalent elements, mainly by Sn (up to 15.88 wt% SnO; 0.228 Sn apfu), to a lesser extent by V (up to 1.89 wt% VO_2; 0.045 V apfu), and by scarcely noticeable Zr (up to 0.43 wt% ZrO_2; 0.007

No. analyses	SP3_3	SP3_28	SP3_30	SP3_25	SP31_271	SP3_32	SP3_31	SP3_7	SP31_275	SP31_281	SP14_131	SP31_277	SP5_4	SP5_7	SP5_2	SP5_3	SP5_1
Nb_2O_5	**0.14**	**b.d.**	**0.16**	**0.39**	**6.58**	**0.38**	**0.57**	**0.83**	**9.85**	**6.19**	**0.40**	**7.59**	**9.17**	**9.06**	**3.64**	**1.70**	**1.80**
Ta_2O_5	**b.d.**	**0.10**	**0.15**	**0.36**	**7.65**	**0.49**	**0.79**	**1.18**	**0.28**	**1.52**	**0.14**	**0.66**	**1.05**	**1.73**	**0.48**	**0.43**	**0.41**
SiO_2	30.46	30.22	30.47	29.68	29.22	29.00	29.33	29.05	27.75	27.60	28.76	27.30	23.77	23.11	24.17	21.14	23.08
TiO_2	25.39	22.13	24.50	25.97	19.48	26.08	27.15	27.71	17.21	18.62	23.73	17.77	14.15	11.40	14.03	0.65	0.64
VO_2	1.71	0.10	0.10	0.12	0.26	0.18	0.12	0.09	0.27	0.18	0.09	0.26	–	–	–	–	–
ZrO_2	b.d.	b.d.	b.d.	0.11	0.36	0.12	0.12	0.11	0.19	0.24	b.d.	0.18	b.d.	0.06	0.11	b.d.	b.d.
SnO_2	**b.d.**	**0.52**	**1.13**	**4.91**	**5.81**	**6.79**	**7.16**	**9.91**	**12.55**	**14.41**	**14.78**	**15.88**	**19.52**	**25.68**	**28.70**	**50.25**	**50.40**
Al_2O_3	7.41	9.27	8.22	4.68	3.86	3.71	3.13	1.81	2.97	2.00	3.47	2.03	0.18	0.04	0.03	b.d.	b.d.
Sc_2O_3	0.43	0.20	0.21	0.96	0.27	0.57	0.54	0.09	0.91	1.90	b.d.	1.23	–	–	–	b.d.	b.d.
Fe_2O_3	1.21	1.21	1.18	1.26	1.39	1.29	1.29	1.10	1.41	1.18	0.66	1.32	5.08	2.94	2.49	2.85	2.85
Y_2O_3	**5.03**	**6.83**	**3.94**	**3.50**	**b.d.**	**3.12**	**2.38**	**0.98**	**b.d.**	**b.d.**	**b.d.**	**b.d.**	**b.d.**	**b.d.**	**0.04**	**b.d.**	**b.d.**
Ce_2O_3	b.d.	b.d.	b.d.	b.d.	b.d.	b.d.	b.d.	b.d.	b.d.	b.d.	b.d.	b.d.	0.10	0.13	0.09	–	–
Gd_2O_3	0.32	b.d.	b.d.	b.d.	b.d.	b.d.	b.d.	b.d.	b.d.	b.d.	b.d.	b.d.	–	–	–	–	–
Dy_2O_3	0.24	0.33	0.14	0.21	b.d.	0.13	0.07	b.d.	b.d.	b.d.	b.d.	b.d.	–	–	–	–	–
Ho_2O_3	b.d.	0.18	0.18	0.19	0.18	0.13	0.22	0.17	0.20	0.16	0.11	0.15	–	–	–	–	–
Er_2O_3	0.36	0.51	0.26	0.26	b.d.	0.23	0.18	0.07	b.d.	b.d.	b.d.	b.d.	–	–	–	–	–
Tm_2O_3	0.07	0.06	b.d.	b.d.	0.08	b.d.	b.d.	b.d.	b.d.	b.d.	b.d.	b.d.	–	–	–	–	–
Yb_2O_3	0.76	1.03	0.59	0.35	b.d.	0.32	0.23	0.08	b.d.	b.d.	b.d.	b.d.	–	–	–	–	–
Lu_2O_3	0.19	0.24	0.12	0.11	b.d.	0.08	b.d.	b.d.	b.d.	b.d.	b.d.	b.d.	–	–	–	–	–
MnO	0.09	0.05	0.08	0.04	b.d.	0.03	b.d.	0.04	b.d.	b.d.	0.06	b.d.	0.10	0.11	0.18	0.19	0.16
CaO	24.84	23.60	25.56	25.44	26.28	25.26	25.67	26.29	26.45	26.34	26.97	26.11	23.95	22.33	23.11	21.07	21.17
MgO	0.15	0.35	0.15	0.10	b.d.	0.05	0.05	b.d.	b.d.	b.d.	b.d.	b.d.	–	–	–	b.d.	b.d.
Na_2O	–	–	–	–	–	–	–	–	–	–	–	–	0.45	0.87	0.18	b.d.	b.d.
F	1.38	1.91	1.82	0.97	0.20	0.69	0.45	0.31	0.18	0.34	0.75	0.27	–	–	–	–	–
$H_2O_{(calc.)}$	0.53	0.68	0.68	0.57	0.00	0.51	0.46	0.20	0.23	0.25	0.67	0.11	0.33	0.17	0.13	0.51	0.14
-O = F2	-0.58	-0.81	-0.76	-0.41	-0.08	-0.29	-0.19	-0.13	-0.08	-0.14	-0.31	-0.11	0.00	0.00	0.00	0.00	0.00
Total	100.12	98.70	98.88	99.76	101.54	98.88	99.71	99.88	100.35	100.78	100.27	100.74	97.85	97.63	97.39	98.79	100.65
(atom per formula unit)																	
X-site																	
Y^{3+}	0.088	0.122	0.070	0.063	0.000	0.057	0.044	0.018	0.000	0.000	0.000	0.000	0.000	0.000	0.001	0.000	0.000
Ce^{3+}	0.000	0.000	0.000	0.000	0.000	0.000	0.000	0.000	0.000	0.000	0.000	0.000	0.001	0.002	0.001	–	–
Gd^{3+}	0.003	0.000	0.000	0.000	0.000	0.000	0.000	0.000	0.000	0.000	0.000	0.000	–	–	–	–	–
Dy^{3+}	0.003	0.004	0.001	0.002	0.000	0.001	0.001	0.000	0.000	0.000	0.000	0.000	–	–	–	–	–
Ho^{3+}	0.000	0.002	0.002	0.002	0.002	0.001	0.002	0.002	0.002	0.002	0.001	0.002	–	–	–	–	–
Er^{3+}	0.004	0.005	0.003	0.003	0.000	0.002	0.002	0.001	0.000	0.000	0.000	0.000	–	–	–	–	–
Tm^{3+}	0.001	0.001	0.000	0.000	0.001	0.000	0.000	0.000	0.000	0.000	0.000	0.000	–	–	–	–	–
Yb^{3+}	0.008	0.011	0.006	0.004	0.000	0.003	0.002	0.001	0.000	0.000	0.000	0.000	–	–	–	–	–
Lu^{3+}	0.002	0.002	0.001	0.001	0.000	0.001	0.000	0.000	0.000	0.000	0.000	0.000	–	–	–	–	–
Mn^{2+}	0.002	0.001	0.002	0.001	0.000	0.001	0.000	0.001	0.000	0.000	0.002	0.000	0.003	0.004	0.006	0.007	0.006
Ca^{2+}	0.875	0.848	0.908	0.923	0.988	0.936	0.944	0.977	1.011	1.010	1.004	1.009	0.996	0.963	0.987	1.005	0.979
Na^{+}	–	–	–	–	–	–	–	–	–	–	–	–	0.034	0.068	0.014	0.000	0.000
ΣX-site	0.98	1.00	0.99	1.00	0.99	1.00	0.99	1.00	1.01	1.01	1.01	1.01	1.03	1.04	1.01	1.01	0.98
Y-site																	
Nb^{5+}	0.002	0.000	0.002	0.006	0.104	0.006	0.009	0.013	0.159	0.100	0.006	0.124	0.161	0.165	0.066	0.034	0.035
Ta^{5+}	0.000	0.001	0.001	0.003	0.073	0.005	0.007	0.011	0.003	0.015	0.001	0.007	0.011	0.019	0.005	0.005	0.005
Ti^{4+}	0.628	0.558	0.611	0.662	0.514	0.678	0.701	0.723	0.462	0.501	0.620	0.482	0.413	0.345	0.421	0.022	0.021
V^{4+}	0.045	0.003	0.003	0.003	0.007	0.005	0.003	0.002	0.008	0.005	0.003	0.007	–	–	–	–	–
Zr^{4+}	0.000	0.000	0.000	0.002	0.006	0.002	0.002	0.002	0.003	0.004	0.000	0.003	0.000	0.001	0.002	0.000	0.000
Sn^{4+}	0.000	0.007	0.015	0.066	0.081	0.094	0.098	0.137	0.179	0.206	0.205	0.228	0.302	0.412	0.456	0.891	0.867
Al^{3+}	0.287	0.366	0.321	0.187	0.160	0.151	0.127	0.074	0.125	0.084	0.142	0.086	0.008	0.002	0.001	0.000	0.000
Sc^{3+}	0.012	0.006	0.006	0.028	0.008	0.017	0.016	0.003	0.028	0.059	0.000	0.039	–	–	–	0.000	0.000
Fe^{3+}	0.030	0.031	0.029	0.032	0.037	0.034	0.033	0.029	0.038	0.032	0.017	0.036	0.148	0.089	0.075	0.096	0.093

No. analyses	SP3_3	SP3_28	SP3_30	SP3_25	SP31_271	SP3_32	SP3_31	SP3_7	SP31_275	SP31_281	SP14_131	SP31_277	SP5_4	SP5_7	SP5_2	SP5_3	SP5_1
Mg^{2+}	0.007	0.017	0.007	0.005	0.000	0.003	0.003	0.000	0.000	0.000	0.000	0.000	–	–	–	0.000	0.000
ΣY-site	1.01	0.99	1.00	0.99	0.99	0.99	1.00	0.99	1.00	1.01	0.99	1.01	1.04	1.03	1.03	1.048	1.020
Si^{4+}	1.00	1.01	1.01	1.01	1.03	1.00	1.01	1.01	0.99	0.99	1.00	0.98	0.922	0.930	0.964	0.940	0.996
O^{2-}	4.72	4.68	4.70	4.79	4.97	4.82	4.86	4.91	4.92	4.90	4.82	4.93	4.91	4.96	4.96	4.92	4.98
OH^-	0.14	0.11	0.11	0.10	0.00	0.10	0.09	0.06	0.05	0.06	0.10	0.03	0.09	0.04	0.04	0.08	0.02
F^-	0.14	0.20	0.19	0.10	0.02	0.08	0.05	0.03	0.02	0.04	0.08	0.03	–	–	–	–	–

Table 1. Representative chemical compositions of the Szklarska Poręba titanites (wt.% and apfu). Notes: W, La, Ce, Pr, Nd, Sm, Eu, Tb, Pb, U, Th were below the detection limit.

Zr apfu). In the specimen SP5, SnO_2 was present in amounts ranging 13.15–28.70 wt% (0.196–0.456 Sn apfu), locally reaching a prevalence over Ti corresponding to the species malayaite $CaSn(SiO_4)O$. Trivalent Al, Fe and Sc are the main substituents for the $^{Y}R^{4+}$ occupants: 0.70–10.88 wt% Al_2O_3 (0.028–0.406 Al apfu), 0.07–5.99 wt% Fe_2O_3 (0.002–0.151 Fe apfu), and to 1.90 wt% Sc_2O_3 (0.059 Sc apfu). In contrast, in more Sn-enriched titanite crystals of the SP5 specimen, trivalent substituents were dominated by Fe^{3+} (1.74–3.55 wt% Fe_2O_3; 0.075–0.148 Fe apfu), while Al content was subordinate (0.03–0.42 Al_2O_3; 0.001–0.019 Al apfu). The $Al/(Al + Fe^{3+})$ ratio ranges from 0.27 to 0.99, and in Sn-bearing titanite and malayaite of SP5 specimen from 0.01 to 0.12. Besides the substitution $^{X}Ca^{2+} + {}^{Y}Ti^{4+} = {}^{X}REE^{3+} + {}^{Y}(Al, Fe, Sc)^{3+}$ mentioned above, the trivalent Y-site occupants result from two other substitutions: $^{Y}Ti^{4+} + {}^{Z}O^{2-} = {}^{Y}(Al, Fe, Sc)^{3+} + {}^{Z}(F, OH)^-$ and $2^{Y}Ti^{4+} = {}^{Y}(Al, Fe, Sc)^{3+} + {}^{Y}(Nb, Ta)^{5+}$. The co-variation (F + OH) *vs*

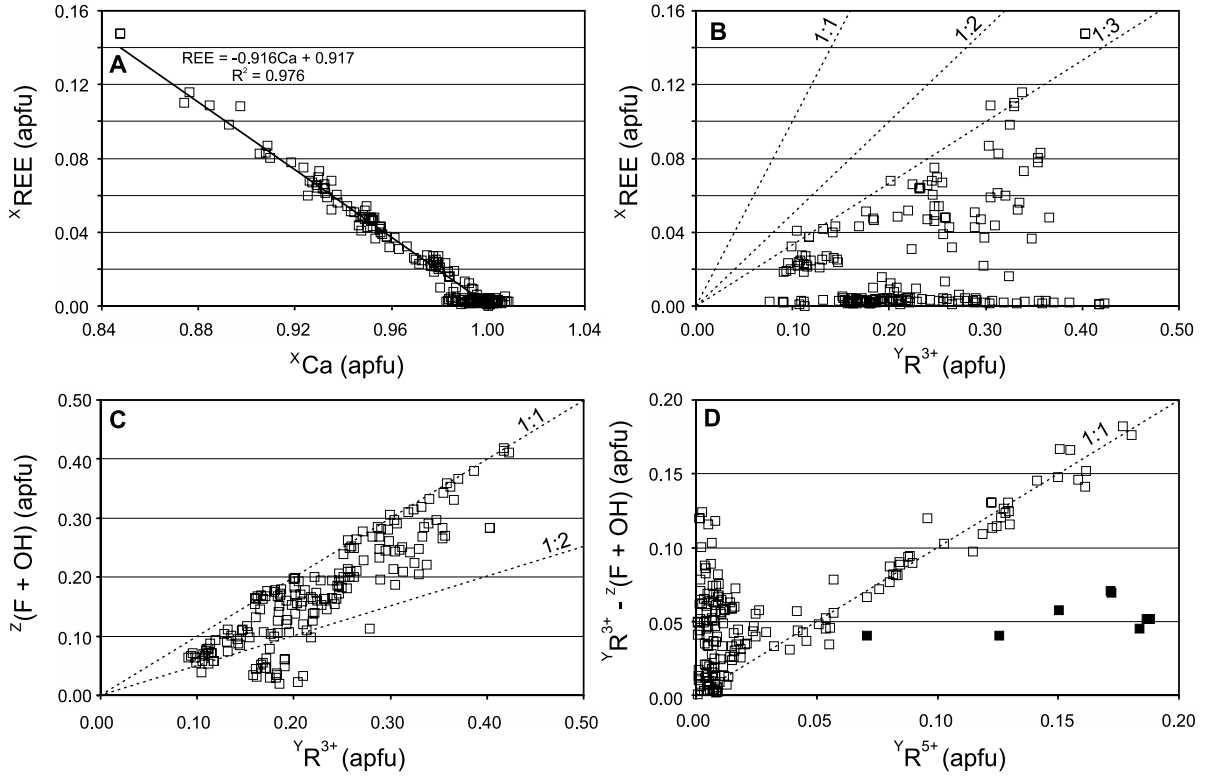

Text-fig. 3. Compositional relationships in the Szklarska Poręba Huta titanite: (A) ^{X}REE *vs* ^{X}Ca; (B) ^{X}REE *vs* $^{Y}R^{3+}$; (C) $^{Z}(F + OH)$ *vs* $^{Y}R^{3+}$; (D) $^{Y}R^{3+} - {}^{Z}(F + OH)$ *vs* $^{Y}R^{5+}$. $^{Y}R^{3+} = Al + Fe^{3+} + Sc$; $^{Y}R^{5+} = Nb + Ta$. All data are presented in atoms per formula unit. Black continuous line – statistical trends, dashed line – 1:1, 1:2, or 1:3 trends between the selected groups of constituents. Full squares at (d) correspond to the titanite-malayaite data collected in specimen SP5.

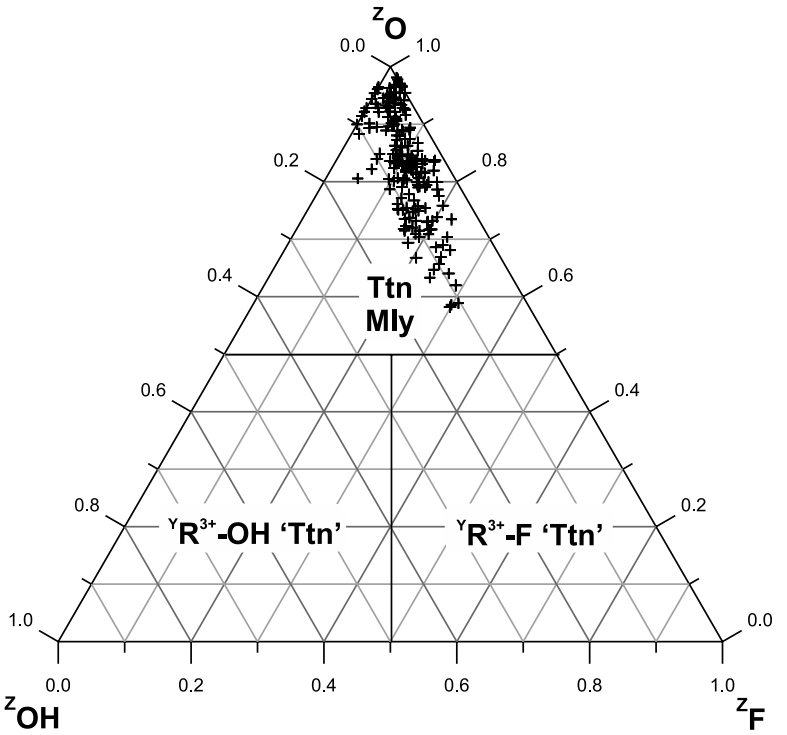

Text-fig. 4. Position of the studied titanites in the ^{Z}(O-F-OH) system.

$^{Y}R^{3+}$ (= Al, Fe, Sc) shows the dominant substitution mechanisms (Text-fig. 3C). Most of the data points fall within the range defined by the two lines corresponding to the (F + OH) / $^{Y}R^{3+}$ ratios of 1:1 and 1:2, which indicate the coupled substitutions: ^{Y}(Al, Fe, Sc) ^{Z}(F, OH)$^{Y}Ti_{-1}{}^{Z}O_{-1}$, and ^{Y}(Al, Fe, Sc)$_2{}^{Y}$(Nb, Ta) ^{Z}(F, OH)$_{-}{}^{Y}Ti_{-3}{}^{Z}O_{-1}$. The data below the 1:2 line indicate compositions with negligible ^{Z}(F, OH), where some amount of ^{Y}(Al, Fe, Sc) occupancy may result from $^{Y}R^{3+} + {}^{Y}R^{5+} = 2\ {}^{Y}Ti^{4+}$ substitution.

The co-variation $^{Y}R^{3+} - {}^{Z}$(OH + F) *vs* (Nb, Ta)$^{5+}$ (Text-fig. 3D) reveals two different substitution mechanisms for the introduction of pentavalent Nb^{5+} and Ta^{5+} into the titanite structure. Typically, these cations enter the structure *via* the substitution $^{Y}R^{3+} + {}^{Y}R^{5+} = 2\ {}^{Y}Ti^{4+}$ (a line with the 1:1 $^{Y}R^{3+}/{}^{Y}R^{5+}$ ratio in Text-fig. 3D). However, the arrangement of data points from Sn-bearing titanite and malayaite from specimen SP5 suggests a substitution mechanism independent of the $^{Y}R^{3+}$ content. This could imply an alternative substitution, for example, related to the presence of divalent Y-site occupants: $^{Y}Fe^{2+} + 2\ {}^{Y}$(Nb, Ta)$^{5+} = 3\ {}^{Y}Ti^{4+}$, or direct substitution for the deficient Si detected in these crystals. The F/(F+OH) varies widely from 0.10–1.00, with F^- generally predominant over OH^-. Text-figure 4 illustrates the classification of the Szklarska Poręba Huta titanites in the ^{Z}(O-OH-F) system. All of them represent titanite evolving into F,Al-bearing titanite, and Sn-bearing analyses collected in the SP5 specimen, either Sn-bearing titanite (Ti > Sn) or Ti-bearing malayaite (Sn > Ti).

GENETIC IMPLICATIONS

The pegmatites exposed in the Szklarska Poręba Huta quarry belong to the NYF (Nb-Y-F) petrogenetic family in the pegmatite classification by Černý and Ercit (2005). In the latest classification system of granitic pegmatites (Wise *et al.* 2022), these pegmatites are related to the products of residual melts from granite magmatism (RMG). However, despite the I-type to transitional I/S type signature of the Karkonosze granite magmas (Duthou *et al.* 1991; Wilamowski 1998; Oberc-Dziedzic *et al.* 1999; Mazur *et al.* 2007; Mikulski 2007; Słaby and Martin 2008), the presence of prominent accessory minerals – such as biotite, magnetite, ilmenite, fergusonite-(Y), gadolinite-(Y), allanite-(Ce), monazite-(Ce), xenotime-(Y), and others – indicate Group 2 RMG pegmatites enriched in Y, Ln, Be, Fe, Ti, Nb, Ta, and P, suggesting the A-type granite affiliation. The two distinct assem-

blages of ore mineralization – Th-U-REE and W-Sn-Mo-Bi – are mainly attributed to apophyses of highly fractionated and evolved fine-grained aplogranite. These apophyses penetrate the porphyritic / central granite in the northwest part of the quarry, enriching the post-magmatic pneumatolytic and hydrothermal system with some of these elements.

Titanite, an accessory mineral of the Szklarska Poręba Huta pegmatite, shows marked compositional heterogeneity. However, most of its crystals share the same inventory of ^{X}Ca and ^{Y}Ti substituents: Y + Ln, Al, Fe^{3+}, Sc, Sn, Nb + Ta, and F and OH replacing ^{Z}O. The observed differentiation in the concentration of these elements likely results from their local and / or temporal concentrations in the fluid-hydrothermal system, which progressively decrease with the temperature. For example, Franz and Spear (1985) suggested that high total pressure and low temperature favour Al for Ti substitution, although their conclusion refers to aluminous titanite in the eclogite zone. Alternatively, Markl and Piazolo (1999) concluded that the chemical composition of Al-bearing titanite is not only a complex function of *P* and *T*, but, more importantly, a function of the composition of the coexisting fluid phase in terms of the H_2O/HF fugacity ratio, and the composition of the host rock in terms of its Al_2O_3/TiO_2 activity ratio. At Szklarska Poręba, the typical crystallization environment for REE-bearing titanite is associated with gadolinite-(Y) and hingganite-(Y), indicating high local concentrations of Y + HREE charge-balanced by the replacement of trivalent Y-site cations (mainly Al + subordinate Fe^{3+} and Sc) for Ti: $(Y, HREE)^{3+} + (Al, Fe, Sc)^{3+} \rightarrow {}^{X}Ca^{2+} + {}^{Y}Ti$. With decreasing local REE concentrations, e.g. due to the occurrence in different mineral associations, other substitution mechanisms $(Al, Fe, Sc)^{3+} + (OH, F)^{-} \rightarrow {}^{Y}Ti + {}^{Z}O$ and $(Al, Fe, Sc)^{3+} + (Nb, Ta)^{5+} \rightarrow 2^{Y}Ti$ start to play the dominant role.

The increasing role of tin in the Szklarska Poręba pneumatolytic-hydrothermal system is evidenced by the crystallization of cassiterite. These cassiterite crystals are often deficient in typical tin substituents like Nb, Ta, Fe, Mn, W, and Ti (usually total < 0.5 wt%), and thus having a composition typical of high-temperature pneumatolytic-hydrothermal cassiterite (AP, *unpublished data*). Higher-temperature Nb + Ta oxides (fergusonite, nioboheftetjernite, columbite) contain only minor Sn. Fluid inclusion studies on this cassiterite indicate that it crystallized at temperatures of 515–470°C (Kozłowski *et al.* 2002), consistent with typical pneumatolytic to high-temperature hydrothermal conditions. In the titanites mentioned above, the Sn content is typically minor, ranging from a few to a dozen wt% SnO_2. However, in sample SP5, which represents the silesiaite and kozłowskiite holotype (Pieczka *et al.* 2022, 2023), more Sn-enriched titanite crystals with up to 28.70 wt% SnO_2 (~0.46 Sn apfu) have been found. Some of them reach compositions corresponding to malayaite $CaSn(SiO_4)O$. In this sample, which is a fragment of a quartz vein cutting aplogranite, titanite and malayaite are associated among others by chalcopyrite, pyrite, bismuthinite, fersmite, Sc-bearing columbite-(Mn), kristiansenite, silesiaite, kozłowskiite, and green andradite, in majority indicating the crystallization of high- to moderate-temperature hydrothermal fluids poor in Al^{3+}. On the eastern side of the Karkonosze granite massif, malayaite has been detected in disseminated polymetallic mineralization hosted by metamorphic calc-silicate rocks in the Rędziny dolomite marble quarry (Pieczka *et al.* 2009). The mineralization consists of high-to medium-temperature pyrrhotite, arsenopyrite, hematite, cassiterite (412–285°C; Mochnacka *et al.* 2001), chalcopyrite, other base-metal sulphides, numerous Ag(Cu)-Pb-Bi-sulphosalts, Bi sulphides, sulphoselenides and tellurides, bismuth and Sn-sulphides of the stannite group, chatkalite, stannoidite, and mawsonite (Pieczka *et al.* 2009). Undoubtedly, ore mineralization in both localities corresponds to similar post-magmatic activity stages associated with the Karkonosze granite intrusion. In the case of the Szklarska Poręba locality, the mineralization shows characteristics typical of pegmatite conditions, evolving towards high-temperature hydrothermal, overprinted by lower-temperature hydrothermal sulphide and quartz + chlorite + zeolite mineralization in small nests in aplogranite. In turn, the ore assemblage of Rędziny represents almost exclusively continuous hydrothermal ore mineralization, ranging from high to low temperatures.

The fluid systems related to ore mineralization in both localities show differentiation. Studies of the homogenization temperatures of fluid inclusions in the Rędziny cassiterite indicated crystallization at temperatures of 412–285°C and pressures of 0.9–0.8 kbar from acid hydrothermal solutions containing dissolved NaCl with small admixtures of $CaCl_2$ (Mochnacka *et al.* 2001). In the case of the Szklarska Poręba melt-fluid system, the fluoride anion played a more important role. Fluorine has been detected, at least in concentrations of ~1 wt% in schorlitic tourmaline, unrecognized REE-bearing fluoro-carbonates and silicates (up to ~4 wt%), and in titanite itself (up to ~3 wt%). Kozłowski and Matyszczak (2022) characterized the parental magma of the

Karkonosze intrusion as F-poor and concluded that the early post-magmatic fluids preserved in secondary inclusions in magmatic quartz were also F-poor. As sources of the F-bearing fluids that migrated into the pluton, the authors consider rock complexes of the metamorphic envelope, including fluorite veins and metasomatites.

The presence of Sc as an accessory constituent in the Szklarska Poręba mineralization suggests a mechanism for the enrichment of the aplogranite magma with certain metallic elements. Scandium is an incompatible element in mantle-derived felsic melts. It can be concentrated to economic levels by magmatic and/or fluid-mediated processes in a variety of rock types at temperatures ranging from magmatic to ambient (Williams-Jones and Vasyukova 2018). Scandium is highly immobile, characterized by very low $D_{Sc}^{fluid/mineral}$ partition coefficients ranging from 0.01 to 0.10 (Kessel *et al.* 2005; Rustioni *et al.* 2021). Experimental evidence shows that scandium, like the other REE, partitions very strongly into the fluoride liquid (Shchekina and Gramenitskii 2008). F-bearing fluids are the most efficient complexing agents in mobilization of Sc, which forms very stable fluoride complexes with the element that can migrate in pegmatites and high-temperature post-magmatic metasomatic rocks like greisens, skarns, and albitized granites (Gramaccioli *et al.* 2000; Shchekina and Gramenitskiy 2008). Gramaccioli *et al.* (2000) and Williams-Jones and Vasyukova (2018) suggest that other Sc complexes such as those with hydroxyls, carbonates, and even chlorides may play an important role in the mobilization and transport of Sc. High-temperature fluids containing F^-, Cl^-, and OH^- are reported to be the most effective agents in the mobilization, transport, fractionation, and deposition of REE species, forming complexes with these elements, that are only slightly less stable than the Sc complexes (Gieré 1990; Gramaccioli *et al.* 2000; Jiang *et al.* 2005; Migdisov and Williams-Jones 2014; Williams-Jones 2015; Migdisov *et al.* 2016). However, due to the dominant abundance of Cl^- in natural melt-fluid systems, the chloride complexes are mainly responsible for the transport of Sc, REE, and many other rare metals, e.g. Nb, Ta, Sn, etc. The presence of Sc in the Szklarska Poręba aplogranite melt-fluid system indicates that the system was open, and at least a portion of the metallic elements enriching the aplogranite could have an external source in the metamorphic envelope of the granite from where they could be mobilized by F, Cl, OH-bearing fluids migrating into the late pegmatite-forming magmas.

CONCLUSIONS

Titanite is an accessory mineral found in granitic pegmatite and ore-mineralized hydrothermal quartz veins cutting aplogranite exposed in Szklarska Poręba Huta quarry. The chemical composition of this mineral was formed by external high-temperature F-bearing fluids, which were released from rock complexes in the metamorphic envelope adjacent to the intruding granite. These rock complexes include metasomatites and fluorite veins. The fluids mobilized certain components of the metamorphic rock complexes (e.g. Sc, REE, Nb, Ta, …) and transported them, among others, in the form of fluoride complexes, finally enriching the aplogranite magma with some metallic elements. The composition of the titanite which crystallized during the pegmatitic to high-temperature hydrothermal stages, was constrained by local equilibria in the aplogranite melt-fluid system. This dependence was influenced by the H_2O/HF fugacity ratio and the composition of the magma in terms of its Al_2O_3/TiO_2 activity ratio. Therefore, all substitution processes observed in titanite are strongly H_2O/HF or Al_2O_3/TiO_2 dependent: (1) $^{X}REE^{3+} + {}^{Y}(Al, Fe, Sc)^{3+} \rightarrow {}^{X}Ca^{2+} + {}^{Y}Ti^{4+}$, (2) $(Al, Fe, Sc)^{3+} + (OH, F)^{-} \rightarrow {}^{Y}Ti + {}^{Z}O$, and (3) $(Al, Fe, Sc)^{3+} + (Nb, Ta)^{5+} \rightarrow 2^{Y}Ti$. Late Sn-bearing titanite found in ore-mineralized quartz veins is almost free of Al, but markedly enriched in Sn, reaching local compositions corresponding to malayaite.

Acknowledgments

The authors wish to thank Dr Eligiusz Szełęg and an anonymous reviewer for very helpful comments and suggestions, which greatly improved the manuscript. This study was supported by the AGH University of Krakow grant 16.16.140.315. The research project was partly supported by the program "Excellence initiative – reserach university" for the AGH University of Krakow.

REFERENCES

Aleksandrowski, P. and Mazur, S. 2002. Collage tectonics in the northeasternmost part of the Variscan Belt: The Sudetes, Bohemian Massif. *Geological Society, London, Special Publications*, **201**, 237–277.

Alexander, J.B. and Flinter, B.H. 1965. A note on varlamoffite and associated minerals from the Batang Padang district, Perak, Malaya, Malaysia. *Mineralogical Magazine*, **35**, 622–627.

Basso, R., Lucchetti, G., Zefiro, L. and Palenzona, A. 1994.

Vanadomalayaite, $CaVOSiO_4$, a new mineral vanadium analog of titanite and malayaite. *Neues Jahrbuch für Mineralogie Monatshefte*, **11**, 489–498.

Beirau, T., Mihailova, B., Malcherek, T., Paulmann, C., Bismayer, U. and Groat, L.A. 2014. Temperature-induced $P2_1/c$ to $C2/c$ phase transition in partially amorphous (metamict) titanite revealed by Raman spectroscopy. *The Canadian Mineralogist*, **52**, 91–100.

Berg, G. 1913. Die Erzlagerstätten der nördlichen Sudeten. "Zeitschr, zum XII Allgemeinen Deutschen Bergmannstage in Breslau". 47 pp. Beiträge zur Geologie Ostdeutschlands. Breslau.

Bismayer, U., Schmahl, W., Schmidt, C. and Groat, L.A. 1992. Linear birefringence and X-ray diffraction studies of the structural phase transition in titanite, $CaTiSiO_5$. *Physics and Chemistry of Minerals*, **19**, 260–266.

Borkowska, M. 1966. Petrography of the Karkonosze granite. *Geologia Sudetica*, **2**, 7–119. [In Polish with French summary]

Brugger, J. and Gieré, R. 1999. As, Sb, Be and Ce enrichment in minerals from a metamorphosed Fe-Mn deposit, Val Ferrera, eastern Swiss Alps. *The Canadian Mineralogist*, **37**, 37–52.

Cempírek, J., Houzar, S. and Novák, M. 2008. Complexly zoned niobian titanite from hedenbergite skarn at Písek, Czech Republic, constrained by substitution $Al(Nb,Ta)Ti_{-2}$, $Al(F,OH)(TiO)_{-1}$ and $SnTi_{-1}$. *Mineralogical Magazine*, **72**, 1293–1305.

Černý, P. and Ercit, T.S. 2005. The classification of granitic pegmatites revisited. *The Canadian Mineralogist*, **43**, 2005–2026.

Černý, P. and Riva di Sanseverino, L. 1972. Comments on crystal chemistry of titanite. *Neues Jahrbuch für Mineralogie Monatshefte*, **3**, 97–103.

Černý, P., Novák, M. and Chapman, R. 1995. The $Al(Nb,Ta)Ti_{-2}$ substitution in titanite: the emergence of a new species? *Mineralogy and Petrology*, **52**, 61–73.

Chakhmouradian, A.R., Reguir, E.P. and Mitchell, R.H. 2003. Titanite in carbonatitic rocks: Genetic dualism and geochemical significance. *Periodico di Mineralogia*, *Eurocarb Special Issue*, **72**, 107–113.

Clark, A.M. 1974. A tantalum-rich variety of sphene. *Mineralogical Magazine*, **39**, 605–607.

Della Ventura, G., Bellatreccia, F. and Williams, C.T. 1999. Zr- and LREE-rich titanite from Tre Croci, Vico volcanic complex (Latinum, Italy). *Mineralogical Magazine*, **63**, 123–130.

Duthou, J.L., Couturie, J.P., Mierzejewski, M.P. and Pin, C. 1991. Age determination of the Karkonosze granite using the Rb-Sr isochrone whole-rock method. *Przegląd Geologiczny*, **36**, 75–79. [In Polish]

Evans, R.J., Gołębiowska, B., Groat, L.A. and Pieczka, A. 2018. Crystal structure of kristiansenite from Szklarska Poręba, southwestern Poland. *Minerals*, **8**, 584.

Franke, W. and Ghobarkar, H. 1980. The morphology of titanite grown from aqueous supercritical solutions. *Neues Jahrbuch für Mineralogie*, **12** , 564–568.

Franz, G. and Spear, F.S. 1985. Aluminious titanite (sphene) from the Eclogite zone, south-central Tauern Window, Austria. *Chemical Geology*, **50**, 33–46.

Gajda, E. 1960. Minerals of the pegmatite veins of the Szklarska Poręba vicinity. *Kwartalnik Geologiczny*, **4**, 565–584. [In Polish with English summary]

Gieré, R. 1990. Hydrothermal mobility of Ti, Zr and REE: examples from the Bergell and Adamello contact aureoles (Italy). *Terra Nova*, **2**, 60–67.

Gramaccioli, C.M., Diella, V. and Demartin, F. 2000. The formation of scandium minerals as an example of the role of complexes in the geochemistry of rare earths and HFS elements. *European Journal of Mineralogy*, **12**, 795–808.

Higgins, J.B. and Ribbe, P.H. 1976. The crystal chemistry and space group of natural and synthetic titanites. *American Mineralogist*, **61**, 878–888.

Higgins, J.B. and Ribbe, P.H. 1977. The structure of malayaite, $CaSnOSiO_4$, a tin analog of titanite. *American Mineralogist*, **62**, 801–806.

Ilnicki, S. 2011. Amphibolites from the Szklarska Poręba hornfels belt, West Sudetes, SW Poland: Magma genesis and implications for the break-up of Gondwana. *International Journal of Earth Sciences*, **101**, 1253–1272.

Jiang, S.Y., Wang, R.C., Xu, X.S. and Zhao, K.D. 2005. Mobility of high field strength elements (HFSE) in magmatic-, metamorphic-, and submarine-hydrothermal systems. *Physics and Chemistry of the Earth*, **30**, 1020–1029.

Karwowski, Ł., Olszyński, W. and Kozłowski, A. 1973. Wolframite mineralization from the vicinity of Szklarska Poręba Huta. *Przegląd Geologiczny,* **21**, 633–637. [In Polish]

Kek, S., Aroyo, M., Bismayer, U., Schmidt, C., Eichhorn, K. and Krane, H.G. 1997. The two-step phase transition of titanite, $CaTiSiO_5$: a synchrotron radiation study. *Zeitschrift für Kristallographie*, **212**, 9–19.

Kessel, R., Schmidt, M.W., Ulmer, P. and Pettke, T. 2005. Trace element signature of subduction-zone fluids, melts and supercritical liquids at 120–180 km depth. *Nature*, **437**, 724–727.

Kozłowski, A. 1978. Pneumatolytic and hydrothermal activity in the Karkonosze Izera block. *Acta Geologica Polonica*, **28**, 171–222.

Kozłowski, A. 2007. Melt inclusions in quartz from the Karkonosze granitoids. *Archivum Mineralogiae Monograph*, **1**, 147–153.

Kozłowski, A. and Karwowski, Ł. 1975. Genetic indications of the W-Sn-Mo mineralisation in the Karkonosze-Izera area. *Kwartalnik Geologiczny*, **19**, 67–73. [In Polish]

Kozłowski, A. and Matyszczak, W. 2018. Oxygenic bismuth minerals in the NE part of the Karkonosze pluton (West Sudetes, SW Poland). *Acta Geologica Polonica*, **68**, 537–554.

Kozłowski, A. and Matyszczak, W. 2022. Fluorite and related fluids in the Karkonosze granitoid pluton, SW Poland. *Acta Geologica Polonica*, **72**, 9–31.

Kozłowski, A. and Sachabiński, M. 2007. Karkonosze intragranitic pegmatites and their minerals. *Granitoids in Poland, Archivum Mineralogiae Monograph*, **1**, 155–178.

Kozłowski, A., Ilnicki, S., Matyszczak, W. and Marcinowska, A. 2016. Magmatic and post-magmatic phenomena in the Karkonosze granite and its metamorphic envelope (West Sudetes, SW Poland). *Acta Geologica Polonica*, **66**, 451–471.

Kozłowski, A., Karwowski, Ł. and Olszyński, W. 1975. Tungsten-tin-molybdenum mineralization in the Karkonosze massif. *Acta Geologica Polonica*, **25**, 415–430.

Kozłowski, A., Sanocka, M. and Dzierżanowski, P. 2002. Tin-tungsten and associate mineralization at Szklarska Poręba Huta, Karkonosze massif, SW Poland. *Mineralogical Society of Poland, Special Papers*, **20**, 248–250.

Kröner, A., Hegner, E., Hammer, J., Haase, G., Bielicki, K.H., Krauss, M. and Eidam, J. 1994. Geochronology and Nd-Sr systematics of Lusatian granitoids – significance for the evolution of the Variscan orogen in East-Central Europe. *Geologische Rundschau*, **83**, 357–376.

Kryza, R. and Mazur, S. 1995. Contrasting metamorphic paths in the SE part of the Karkonosze-Izera block (Western Sudetes, SW Poland). *Neues Jahrbuch fur Mineralogie-Abhandlungen*, **169**, 157–192.

Kryza, R., Pin, C., Oberc-Dziedzic, T., Crowley, Q.G. and Larionov, A. 2014a. Deciphering the geochronology of a large granitoid pluton (Karkonosze Granite, SW Poland): An assessment of U-Pb zircon SIMS and Rb-Sr whole-rock dates relative to U-Pb zircon CA-ID-TIMS. *International Geology Review*, **56**, 756–782.

Kryza, R., Schaltegger, U., Oberc-Dziedzic, T., Pin, C. and Ovtcharova, M. 2014b. Geochronology of a composite granitoid pluton: a high-precision ID-TIMS U-Pb zircon study of the Variscan Karkonosze Granite (SW Poland). *International Journal of Earth Sciences*, **103**, 683–696.

Kusiak, M.A., Williams, I.S., Dunkley, D.J., Konečny, P., Słaby, E. and Martin, H. 2014. Monazite to the rescue: U-Th-Pb dating of the intrusive history of the composite Karkonosze pluton, Bohemian Massif. *Chemical Geology*, **364**, 76–92.

Liferovich, R.P. and Mitchell, R.H. 2005. Crystal chemistry of titanite-structured compounds: the $CaTi_{1-x}Zr_xOSiO_4$ ($x \leq 0.5$) series. *Physics and Chemistry of Minerals*, **32**, 40–51.

Lussier, A.J., Cooper, M.A., Hawthorne, F.C. and Kristiansen, R. 2009. Triclinic titanite from the Heftetjern granitic pegmatite, Tørdal, Southern Norway. *Mineralogical Magazine*, **73**, 709–722.

Machowiak, K. and Armstrong, R. 2007. SHRIMP U-Pb zircon age from the Karkonosze granite. *Mineralogia Polonica, Special Papers*, **31**, 193–196.

Markl, G. and Piazolo, S. 1999. Stability of high-Al titanite from low pressure calcsilicates in light of fluid and host-rock composition. *American Mineralogist*, **84**, 37–47.

Mazur, S. and Aleksandrowski, P. 2001. The Teplá(?)/Saxothuringian suture in Karkonosze-Izera massif western Sudetes, central European Variscides. *International Journal of Earth Sciences*, **90**, 341–360.

Mazur, S., Aleksandrowski, P., Kryza, R. and Oberc-Dziedzic, T. 2006. The Variscan orogen in Poland. *Geological Quarterly*, **50**, 89–118.

Mazur, S., Aleksandrowski, P., Turniak, K. and Awdankiewicz, M. 2007. Geology, tectonic evolution and Late Palaeozoic magmatism of Sudetes – an overview. *Granitoids in Poland*, *Archivum Mineralogiae Monograph*, **1**, 59–87.

Meyer, H.W., Zhang, M., Bismayer, U., Salje E.K.H., Schmidt, C., Kek, S., Morgenroth, W. and Bleser, T. 1996. Phase transformation of natural titanite: an infrared, Raman spectroscopic, optical birefringence and X-ray diffraction study. *Phase Transitions*, **59**, 39–60.

Migdisov, A. and Williams-Jones, A.E. 2014. Hydrothermal transport and deposition of the rare earth elements by fluorine-bearing aqueous liquids. *Mineralium Deposita*, **49**, 987–997.

Migdisov, A., Williams-Jones, A.E., Brugger, J. and Caporuscio, F.A. 2016. Hydrothermal transport, deposition, and fractionation of the REE: Experimental data and thermodynamic calculations. *Chemical Geology*, **439**, 13–42.

Mikulski, S.Z. 2007. Metal ore potential of the parent magma of granite – the Karkonosze massif example. *Granitoids in Poland, Archivum Mineralogiae Monograph*, **1**, 123–145.

Mikulski, S.Z., Williams, I.S., Stein, H.J. and Wierchowiec, J. 2020. Zircon U-Pb dating of magmatism and mineralizing hydrothermal activity in the Variscan Karkonosze massif and its eastern metamorphic cover SW Poland. *Minerals*, **10**, 1–34.

Mochnacka, K., Oberc-Dziedzic, T., Mayer, W. and Pieczka, A. 2015. Ore mineralization related to geological evolution of the Karkonosze-Izera Massif (the Sudetes, Poland) – Towards a model. *Ore Geology Reviews*, **54**, 215–238.

Mochnacka, K., Pieczka, A., Gołębiowska, B. and Kozłowski, A. 2001. Cassiterite from Rędziny and its relationship to the tin-bearing schist of Izera area (SW Poland). In: Piestrzyński, A. *et al.* (Eds), Mineral Deposits at the Begining of the 21st Century, 457–460. Swets & Zeitlinger Publishers. Lisse-Tokyo.

Oberc-Dziedzic, T., Żelaźniewicz, A. and Cwojdziński, S. 1999. Granitoids of the Odra fault zone: late to post-orogenic Variscan intrusions in the Saxothuringian zone, SW Poland. *Geologia Sudetica*, **32**, 55–71.

Olszyński, W., Kozłowski, A. and Karwowski, Ł. 1976. Bismuth minerals from the Karkonosze massif. *Acta Geologica Polonica*, **26**, 443–449.

Petrascheck, W.E. 1933. Die Erzlagerstätten des Schlesischen Gebirges. *Archiv für Lagerstättenforschung*, **59**, 5–53.

Pieczka, A. and Gołębiowska, B. 2002. Pegmatites of the Szklarska Poręba Huta granite quarry: preliminary data on REE mineralization. *Mineralogical Society of Poland, Special Papers*, **20**, 175–177.

Pieczka, A. and Gołębiowska, B. 2012. Cuprobismutite homologues in granitic pegmatites from Szklarska Poręba, Karkonosze Massif, Southwestern Poland. *The Canadian Mineralogist*, **50**, 313–324.

Pieczka, A., Gołębiowska, B. and Parafiniuk, J. 2009. Conditions of formation of polymetallic mineralization in the eastern envelope of the Karkonosze granite: The case of Rędziny, southwestern Poland. *The Canadian Mineralogist*, **47**, 765–786.

Pieczka, A., Gołębiowska, B., Ilnicki, S., Dzierżanowski, P. and Jeżak, L. 2003. Gadolinite group minerals from Szklarska Poręba (SW Poland, Lover Silesia, Karkonosze Mts). International Symposium on Light Elements in Rock-forming Minerals. Book of abstracts, 61–62. Masaryk University & Moravian Museum, Brno.

Pieczka, A., Hawthorne, F.C., Ma, C. Rossman, G.R., Szełęg, E., Szuszkiewicz, A., Turniak, K., Nejbert, K., Ilnicki, S.S., Buffat, P. and Rutkowski, B. 2017. Żabińskiite, ideally $Ca(Al_{0.5}Ta_{0.5})(SiO_4)O$, a new mineral of the titanite group from the Piława Górna pegmatite, the Góry Sowie Block, southwestern Poland. *Mineralogical Magazine*, **81**, 591–610.

Pieczka, A., Zelek-Pogudz, S., Gołębiowska, B., Stadnicka, K.M. and Evans, R.J. 2022. Kozłowskiite, ideally $Ca_4Fe^{2+}Sn_3(Si_2O_7)_2(Si_2O_6OH)_2$, a new kristiansenite-type mineral from Szklarska Poręba, Lower Silesia, Poland. *Mineralogical Magazine*, **86**, 507–517.

Pieczka, A., Zelek-Pogudz, S., Gołębiowska, B., Stadnicka, K.M. and Kristiansen, R. 2023. Silesiaite, ideally $Ca_2Fe^{3+}Sn(Si_2O_7)(Si_2O_6OH)$, a new species in the kristiansenite group: crystal chemistry and structure of holotype silesiaite from Szklarska Poręba, Poland, and Sc-free silesiaite from Häiviäntien, Finland. *Mineralogical Magazine*, **87**, 1–37.

Ribbe, P.H. 1980. Titanite. *Reviews in Mineralogy*, **5**, 137–154.

Rustioni, G., Audetat, A. and Keppler, H. 2021. The composition of subduction zone fluids and the origin of the trace element enrichment in arc magma. *Contributions to Mineralogy and Petrology*, **176**, 51.

Shchekina, T.I., and Gramenitskii, E.N. 2008. Geochemistry of Sc in the magmatic process: Experimental evidence. *Geochemistry International*, **46**, 351–366.

Słaby, E. and Martin, H. 2008. Mafic and felsic magma interaction in granites: the Hercynian Karkonosze pluton (Sudetes, Bohemian Massif). *Journal of Petrology*, **49**, 353–391.

Speer, J.A. and Gibbs, G.V. 1976. The crystal structure of synthetic titanite, $CaTiOSiO_4$, and the domain textures of natural titanites. *American Mineralogist*, **61**, 238–247.

Stepanov, A.V., Bekenova, G.K., Levin, V.L. and Hawthorne, F.C. 2012. Natrotitanite, ideally $(Na_{0.5}Y_{0.5})Ti(SiO_4)O$, a new mineral from the Verkhnee Espe deposit, Akjailyautas mountains, Eastern Kazakhstan district, Kazakhstan: description and crystal structure. *Mineralogical Magazaine*, **76**, 39–44.

Tiepolo, M., Oberti, R. and Vanucci, R. 2002. Trace-element incorporation in titanite: constraints from experimentally determined solid/liquid partition coefficients. *Chemical Geology*, **191**, 105–119.

Warr, L.N. 2021. IMA-CNMNC approved mineral symbols. *Mineralogical Magazine*, **85**, 291–320.

Wilamowski, A. 1998. Geotectonic environment of the Karkonosze and Tatra granite intrusions based on geochemical data. *Archiwum Mineralogiczne*, **51**, 261–271. [In Polish]

Williams-Jones, A.E. 2015. The hydrothermal mobility of the rare earth elements. In: Simandl, G.J. and Neetz, M. (Eds.), Symposium on Strategic and Critical Materials Proceedings, 119–123. British Columbia Geological Survey Paper; Victoria, British Columbia.

Williams-Jones, A.E. and Vasyukova, O.V. 2018. The economic geology of scandium, the runt of the rare earth element litter. *Economic Geology*, **113**, 973–988.

Wise, M.A., Müller, A. and Simmons, W.B. 2022. A proposed new mineralogical classification system for granitic pegmatites. *The Canadian Mineralogist*, **60**, 229–248.

Zachariasen, W.H. (1930) The crystal structure of titanite. *Zeitschrift für Kristallographie,* **73**, 7–16.

Žák, J., Verner, K., Sláma, J., Kachlík, V. and Chlupáčová, M. 2013. Multistage magma emplacement and progressive strain accumulation in the shallow-level Krkonoše-Jizera plutonic complex, Bohemian Massif. *Tectonics*, **32**, 1493–1512.

Zhang, M., Salje, E.K.H., Bismayer, U., Unruh, H.G., Wruck, B. and Schmidt, C. 1995. Phase transition(s) in titanite $CaTiSiO_5$: an infrared spectroscopic, dielectric response and heat capacity study. *Physics and Chemistry of Minerals*, **22**, 41–49.

Manuscript submitted: 5th April 2024
Revised version accepted: 12th August 2024